

Comparison of Scheimpflug imaging and spectral domain anterior segment optical coherence tomography for detection of narrow anterior chamber angles

DS Grewal^{1,2}, GS Brar¹, R Jain¹ and SPS Grewal¹

CLINICAL STUDY

Abstract

Purpose To compare the performance of anterior chamber volume (ACV) and anterior chamber depth (ACD) obtained using Scheimpflug imaging with angle opening distance (AOD500) and trabecular-iris space area (TISA500) obtained using spectral domain anterior segment optical coherence tomography (SD-ASOCT) in detecting narrow angles classified using gonioscopy.

Methods In this prospective, cross-sectional observational study, 265 eyes of 265 consecutive patients underwent sequential Scheimpflug imaging, SD-ASOCT imaging, and gonioscopy. Correlations between gonioscopy grading, ACV, ACD, AOD500, and TISA500 were evaluated. Area under receiver operating characteristic curve (AUC), sensitivity, specificity, and likelihood ratios (LRs) were calculated to assess the performance of ACV, ACD, AOD500, and TISA500 in detecting narrow angles (defined as Shaffer grade ≤ 1 in all quadrants). SD-ASOCT images were obtained at the nasal and temporal quadrants only.

Results Twenty-eight eyes (10.6%) were classified as narrow angles on gonioscopy. ACV correlated with gonioscopy grading ($P < 0.001$) for temporal ($r = 0.204$), superior ($r = 0.251$), nasal ($r = 0.213$), and inferior ($r = 0.236$) quadrants. ACV correlated with TISA500 for nasal ($r = 0.135$, $P = 0.029$) and temporal ($P = 0.160$, $P = 0.009$) quadrants and

also with AOD500 for nasal ($r = 0.498$, $P < 0.001$) and temporal ($r = 0.517$, $P < 0.001$) quadrants. For detection of narrow angles, ACV (AUC = 0.935; 95% confidence interval (CI) = 0.898–0.961) performed similar to ACD (AUC = 0.88, $P = 0.06$) and significantly better than AOD500 nasal (AUC = 0.761, $P = 0.001$), AOD500 temporal (AUC = 0.808, $P < 0.001$), TISA500 nasal (AUC = 0.756, $P < 0.001$), and TISA500 temporal (AUC = 0.738, $P < 0.001$). Using a cutoff of 113 mm³, ACV had 90% sensitivity and 88% specificity for detecting narrow angles. Positive and negative LRs for ACV were 8.63 (95% CI = 7.4–10.0) and 0.11 (95% CI = 0.03–0.4), respectively.

Conclusions ACV measurements using Scheimpflug imaging outperformed AOD500 and TISA500 using SD-ASOCT for detecting narrow angles.

Eye (2011) 25, 603–611; doi:10.1038/eye.2011.14; published online 18 February 2011

Keywords: scheimpflug imaging; anterior segment OCT; narrow angles; glaucoma

Introduction

Glaucoma affects approximately 67 million people making it the most common cause of irreversible blindness worldwide.¹ Although constituting only about 26% of all glaucoma, primary angle closure glaucoma (PACG) is an aggressive and visually destructive disease,^{2,3}

¹Grewal Eye Institute, Chandigarh, India

²Department of Ophthalmology, Northwestern University Feinberg School of Medicine, Chicago, IL, USA

Correspondence: DS Grewal, Department of Ophthalmology, Northwestern University Feinberg School of Medicine, 645 North Michigan Avenue, Suite 440, Chicago, IL 60611, USA
Tel: +1 312 908 8152;
Fax: +1 312 503 8152.
E-mail: dilraj@gmail.com

Received: 1 July 2010
Accepted in revised form: 11 December 2010
Published online: 18 February 2011

This article was presented in part as a free paper at the American Academy of Ophthalmology Annual Meeting, San Francisco, CA, USA, October 2009.

with estimations that it blinds five times more people than primary open-angle glaucoma⁴ making it an important public health problem. The prevalence of PACG varies among different ethnic groups and is a major form of glaucoma in the populous nations of China⁵ and India.⁶ To effectively prevent PACG by the use of prophylactic laser iridotomy, it is necessary to identify people with anatomically narrow angles.

Anterior segment optical coherence tomography (ASOCT) offers a non-contact method for detecting eyes at risk for angle closure.⁷⁻⁹ Several recent studies have used ASOCT to visualize anterior chamber angle (ACA) structures^{7,10-14} and demonstrated it to be accurate for the detection of closed or occludable angles, with gonioscopy used as the reference.^{7,15,16} Spectral domain ASOCT (SD-ASOCT) technology is faster and more efficient than the conventional time domain ASOCT (TD-ASOCT): by detecting signals from the entire depth range in parallel, rather than serially, it achieves higher speed without losing the signal-to-noise ratio.^{17,18}

Scheimpflug imaging also offers non-contact imaging of the anterior segment. Although Scheimpflug photography cannot fully visualize the entire angle,¹⁹ the software available on the Pentacam Scheimpflug camera (Oculus, Wetzlar, Germany) provides extrapolated measurements of the anterior chamber volume (ACV), which have shown promise in screening for narrow angles.²⁰

The aim of this investigation was to compare the diagnostic performance of Scheimpflug imaging and SD-ASOCT in detecting narrow angles and to evaluate the correlations among the quantitative parameters obtained from these two devices.

Materials and methods

The study was approved by the hospital's Institutional Review Board and adhered to the tenets of the Declaration of Helsinki. Informed consent was obtained from all participants. Patients aged ≥ 40 years were recruited from the comprehensive ophthalmology clinic at Grewal Eye Institute. Patients were excluded if they had a history of glaucoma, intraocular surgery, laser treatment, penetrating trauma, and corneal disorders, such as corneal endothelial dystrophy, corneal opacity, pterygium, or abnormalities that precluded SD-ASOCT or Scheimpflug imaging. All participants underwent best-corrected visual acuity (BCVA) measurement using a logarithm of minimum-angle-of-resolution chart (logMAR chart, Lighthouse Inc., Long Island, NY, USA), auto-refraction (Topcon RM-8000B, Topcon Corporation, Tokyo, Japan), slit-lamp examination (Model BQ 900, Haag-Streit, Bern, Switzerland), stereoscopic optic-disc examination with a 78-diopter lens (Volk Optical Inc.,

Mentor, OH, USA), and intraocular pressure measurement (IOP) using Goldmann applanation tonometry (Haag-Streit, Koniz, Switzerland).

Patients underwent Scheimpflug imaging, SD-ASOCT imaging, and gonioscopy in that order. Scheimpflug and SD-ASOCT imaging were performed in a dark room (~ 1 lux using a digital light meter (Extech 401027 Pocket Digital Light Meter, Extech Instruments, Waltham, MA, USA)) after allowing dark adaptation for 30 s, without the use of any mydriatics, and with the subjects sitting in front of the instrument with their face in an upright position, by a single examiner who was masked to the gonioscopy results. The intensity of light during each examination was measured to standardize the illumination conditions. Manufacturer-recommended quality criteria for image acquisition were used as guidelines for acceptance of scan images.

We certify that all applicable institutional and governmental regulations concerning the ethical use of human volunteers were followed during this research.

Scheimpflug imaging

The Pentacam 50 scan image acquisition mode was used, which captures 50 slit images of the anterior segment in 2 s using a rotating Scheimpflug camera. Only images with a Quality Score > 95 were included. The Pentacam software (Software version 1.11, Oculus) configures a three-dimensional model of the anterior segment with the obtained data, and the central anterior chamber depth along the optical axis (ACD, mm), ACA (degrees), and ACV (μl) are computed. The ACV is calculated using an integral calculus, which considers the anterior chamber as a solid bounded by the posterior surface of the cornea (12 mm diameter around the corneal apex), the iris, and the lens.²¹ Pentacam ACA measurements were not used in this study, as their reliability in eyes with narrow angles has been questioned due to the inability of Scheimpflug imaging to visualize the most peripheral part of the iris and base of the ACA.²⁰

Spectral domain anterior segment optical coherence tomography

The RTVue 100 (Optovue Inc., Fremont, CA, USA, software version 4.0) SD-OCT system was used for anterior segment imaging with an auxiliary lens attachment, the corneal adaptor module (CAM). CAM includes adaptor lenses to produce a telecentric scan geometry for corneal imaging and scan patterns, along with the image processing software. The spectrometer is fitted with a high-speed line camera that captures 26 000 axial (A) scans per second using an 830-nm wavelength

light-source providing an axial resolution of 5 μm and a transverse scan resolution of 15 μm .

For this study, anterior segment morphology was assessed with the corneal adaptor module long (CAM-L), using the angle scan protocol, which captured 1×1024 A-scans in 0.04 s. The patient's fixation was directed to the side of the instrument, using an external fixation light, so that the irido-corneal angle was centered in the instrument's field of view. The external fixation target was approximately 20 cm away from the patient's eye. The working distance between CAM-L and the cornea was approximately 13 mm. Two scans of the angle at 3 o'clock and 9 o'clock position were obtained, representing the temporal and nasal quadrants of each eye. In order to obtain images with the corneo-scleral surface perpendicular to the scanning beam, the software provides guide marks on the image acquisition screen. The superior and inferior quadrants were not scanned to avoid potential eyelid obstruction or anterior segment distortion from eyelid manipulation. To achieve a non-accommodated state, the power setting was adjusted according to the patient's refraction. Only images with Scan-Score Index >45 were included. For quantitative analysis, an ophthalmologist (SPSG) marked out the scleral-spur location in the nasal and temporal quadrants, following which the software computed the quantitative analysis. The scleral spur was determined as the point at which there was a change in curvature of the inner surface of the angle wall.²² Parameters measured were: (a) angle opening distance at 500 μm from the scleral spur (AOD500), defined by Pavlin *et al*²³ as the length of a line drawn from the anterior iris to the corneal endothelium perpendicular to a line drawn along the trabecular meshwork at a given distance from the scleral spur and (b) trabecular-iris space area at 500 μm from the scleral spur (TISA500), defined by Radhakrishnan *et al*^{8,16} as a trapezoidal area with the following boundaries: anteriorly, AOD500; posteriorly, a line drawn from the scleral spur perpendicular to the plane of the inner scleral wall to the opposing iris; superiorly, the inner corneo-scleral wall; and inferiorly, the iris surface.

Gonioscopy

All subjects underwent gonioscopy using a Zeiss style four-mirror gonioscopy lens (Ocular Instruments Inc., Bellevue, WA, USA) by a glaucoma specialist (RJ), who was masked to the SD-ASOCT and Scheimpflug images. Gonioscopy examinations (at $\times 16$ magnification) were performed in a dark room (~ 1 lux using digital light meter) using a 1-mm beam reduced to a very narrow slit with minimal illumination to allow adequate visualization of the structures, while taking care to avoid light falling on the pupil or accidental indentation. Slight

tilting of the gonioscopy lens was permitted in an attempt to gain a view over the convexity of the iris. The vertical beam was offset horizontally for assessing the superior and inferior angles, and was offset vertically for the nasal and temporal angles. The procedure was performed without a mydriatic or miotic agent, and a topical anesthetic was applied before examination. Shaffer grading system^{24,25} was used and a narrow angle was defined as Shaffer grade ≤ 1 in all four quadrants.^{16,26}

Statistical analysis

If both eyes were eligible for the study, only the right eyes of the subjects were analyzed. Temporal and nasal angles were analyzed separately for each eye. With the exception of age, other parameters did not conform to a Gaussian distribution ($P < 0.05$; Kolmogorov-Smirnov test with a Lilliefors significance correction). As data was not normally distributed, Mann-Whitney *U*-test for unpaired data was used to determine differences between groups. Bonferroni correction was used to adjust *P*-values for multiple comparisons. The correlation between gonioscopy and ACV measured by Scheimpflug imaging was calculated using the Spearman's correlation coefficient. Sensitivity, specificity, positive likelihood ratio (LR), negative LR, positive predictive value (PPV), negative predictive value (NPV), and the receiver operating characteristic (ROC) curves for each of the SD-ASOCT and Scheimpflug imaging parameters for identifying narrow angles were calculated using gonioscopy as the reference. The area under the ROC curves (AUC) was compared using a nonparametric approach described by DeLong *et al*.²⁷ Optimal cutoff levels were determined using the Youden index (*J*);²⁸⁻³⁰ $J = (\text{sensitivity} + \text{specificity} - 1)$ for all possible cutoff values. The parameter value with the maximum Youden index was used as the cutoff value.

PPV and NPV were calculated using a prevalence of 8% from this study. We also calculated PPV and NPV using population prevalences of 2.75 and 0.88% for PAC and PACG, respectively, as determined by a recent population-based study in India³¹ to assess the performance of ACV. Statistical analysis was carried out using SPSS 17.0 (SPSS, Chicago, IL, USA) and MedCalc version 9.5.0.0 (MedCalc Software, Mariakerke, Belgium). Statistical significance was assumed at the $P < 0.05$ level.

Results

A total of 300 consecutive participants underwent imaging and among them 35 subjects (11.67%) were excluded because of an undetectable scleral spur on SD-ASOCT. None of the patients were excluded because

they could not undergo gonioscopy, SD-ASOCT, or Pentacam examinations. Two hundred and sixty-five eyes of 265 subjects, 136 females (51.3%) and 129 males (48.7%), were included. The mean age was 55.2 ± 5.1 years (range 40–82 years). Mean central corneal thickness (CCT) was $539.9 \pm 37.6 \mu\text{m}$. Twenty-eight eyes (10.6%) were classified as having narrow angles on gonioscopy (Shaffer ≤ 1 in all four quadrants). Table 1 describes the distribution of gonioscopic grades using the Shaffer scale. The mean BCVA was 0.10 ± 0.20 . The mean spherical equivalent of the manifest refraction was -0.53 ± 3.09 diopters (D) and the mean IOP was 16.2 ± 2.8 mm Hg. Table 2 describes the clinical characteristics of the study population. None of the patients had glaucoma. Of the 28 eyes with narrow angles, 4 were PAC and 10 were PAC suspects.

There was a low but significant correlation ($P < 0.001$) between ACV calculated using Scheimpflug imaging and Gonioscopy grading for the temporal ($r = 0.204$), superior ($r = 0.251$), nasal ($r = 0.213$), and inferior angles ($r = 0.236$), and using mean gonioscopy grade ($r = 0.256$). ACV measurements also had a low but significant correlation with SD-ASOCT-derived TISA500 for the

nasal ($r = 0.135$, $P = 0.029$) and temporal ($r = 0.160$, $P = 0.009$) quadrants. (Figure 1) Similarly, there was a moderately positive correlation between ACV and AOD500 for the nasal ($r = 0.498$, $P < 0.001$) and temporal ($r = 0.517$, $P < 0.001$) quadrants (Figure 2). We did not find any correlation between ACV and age, IOP, or CCT ($P > 0.05$ for each).

ROC curves for predicting narrow angles were constructed for ACV, ACD, TISA500, and AOD500 using gonioscopy as the reference (Figure 3). Comparing the sensitivity and specificity at different values of ACV, we found that using a cutoff of 113 mm^3 , ACV had 90% sensitivity and 88.19% specificity in detecting narrow angles with an AUC = 0.935 (95% confidence interval (CI), 0.898–0.761). ACV outperformed AOD500 nasal (AUC = 0.761; 95% CI, 0.705–0.811; $P < 0.001$), AOD500 temporal (AUC = 0.808; 95% CI, 0.755–0.854; $P < 0.001$), TISA500 nasal (AUC = 0.756; 95% CI, 0.7–0.807; $P < 0.001$), and TISA500 temporal (AUC = 0.738; 95%CI, 0.681–0.790; $P < 0.001$) in detecting narrow angles. Although ACV had a higher AUC than ACD (AUC = 0.880; 95% CI, 0.835–0.917), the difference was not significant ($P = 0.06$) (Table 3). The cutoff values and

Table 1 Distribution of gonioscopic grade classified Shaffer scale in the study population ($n = 265$)

Shaffer grade	Superior n (%)	Nasal n (%)	Inferior n (%)	Temporal n (%)
Grade 0	11 (4.2)	11 (4.2)	10 (3.8)	9 (3.4)
Grade 1	17 (6.4)	17 (6.4)	18 (6.8)	19 (7.2)
Grade 2	60 (22.6)	58 (21.9)	60 (23.4)	62 (19.6)
Grade 3	96 (36.2)	103 (38.9)	96 (35.5)	94 (38.5)
Grade 4	81 (30.6)	76 (28.7)	81 (30.6)	81 (31.3)

Table 2 Clinical characteristics of the study population ($n = 265$)

Parameter	Total subjects (n = 265)	Narrow angles (n = 28)	Open angles (n = 237)	P-value
Age (years)	55.3 ± 5.1 (40–82)	56.2 ± 6.5 (40–76)	58.3 ± 5.7 (50–82)	0.323 ^a
Gender				0.515 ^b
Male	129	12	117	
Female	136	16	120	
Autorefractive spherical error (D)	-0.52 ± 3.09 (-7.5 to 5.5)	0.23 ± 1.33 (-5.5 to 5.25)	-0.75 ± 1.43 (-7.5 to 5.5)	$< 0.001^c$
Intraocular pressure (mmHg)	15.1 ± 2.7 (9–24)	15.8 ± 2.4 (10–24)	14.5 ± 2.9 (9–24)	$< 0.001^c$
ACV (mm^3)	141.1 ± 37.6 (58–248)	95.6 ± 20.6 (58–137)	146.5 ± 35.5 (76–248)	$< 0.001^c$
ACD (mm)	2.63 ± 0.42 (1.59–4.16)	2.07 ± 0.38 (1.59–2.86)	2.70 ± 0.38 (1.8–4.16)	$< 0.001^c$
AOD500 nasal (mm)	0.48 ± 0.21 (0.08–0.83)	0.33 ± 0.14 (0.08–0.44)	0.50 ± 0.21 (0.12–0.83)	$< 0.001^c$
AOD500 temporal (mm)	0.49 ± 0.22 (0.09–0.85)	0.30 ± 0.11 (0.09–0.36)	0.51 ± 0.22 (0.12–0.85)	$< 0.001^c$
TISA500 nasal (mm^2)	0.33 ± 0.12 (0.11–0.68)	0.23 ± 0.14 (0.10–0.54)	0.34 ± 0.11 (0.19–0.68)	$< 0.001^c$
TISA500 temporal (mm^2)	0.32 ± 0.12 (0.08–0.68)	0.23 ± 0.14 (0.08–0.54)	0.33 ± 0.12 (0.11–0.68)	$< 0.001^c$

Abbreviations: ACD, anterior chamber depth; ACV, anterior chamber volume; AOD500, angle opening distance at 500 μm from the scleral spur; TISA500, trabecular-iris space area at 500 μm from the scleral spur.

^aIndependent samples *t*-test.

^b χ^2 -test.

^cMann-Whitney *U*-test.

Data represent the mean \pm SD (range), except for gender.

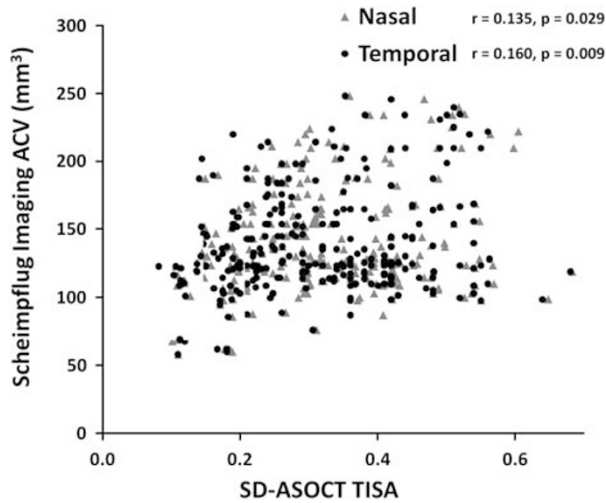


Figure 1 Scatter plot demonstrating correlation of TISA500 (nasal and temporal) versus ACV. TISA, trabecular-iris space area at 500 μm from the scleral spur (mm^2); ACV, anterior chamber volume using Scheimpflug (mm^3); SD-ASOCT, spectral domain anterior segment optical coherence tomography.

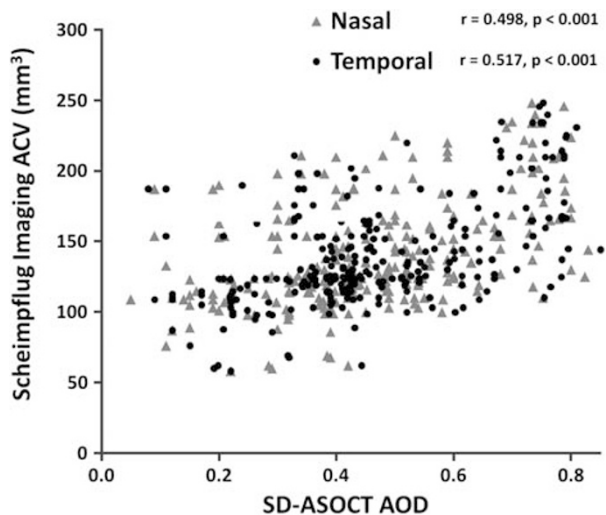


Figure 2 Scatter plot demonstrating correlation of AOD500 (nasal and temporal) versus ACV. AOD, angle opening distance at 500 μm from the scleral spur (mm); ACV, anterior chamber volume using Scheimpflug (mm^3); SD-ASOCT, spectral domain anterior segment optical coherence tomography.

the corresponding sensitivity, specificity, positive LR, negative LR, PPV and NPV for ACV, ACD, AOD500, and TISA500 (nasal and temporal) are presented in Table 3.

Using ACV (with a cutoff of 113 mm^3), the PPV for detecting narrow angles was 42.9% (95% CI, 27.7–59), while the NPV was 99% (95% CI, 96.6–99.9), using an 8% prevalence of narrow angles from this study. The PPV for detecting PAC (using a population prevalence of 2.75%³¹) was 19.6% (95% CI, 7.7–37.8) and the NPV was 99.7%

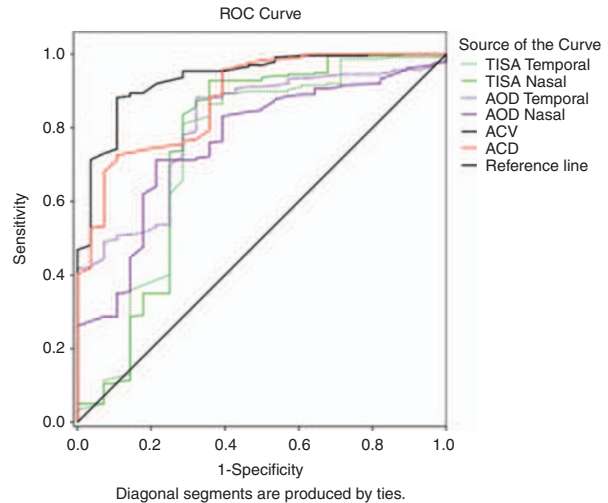


Figure 3 Graph showing receiver operating characteristic curves of different parameters from Scheimpflug imaging (ACV and ACD) and SD-ASOCT (AOD500 and TISA500) of detecting narrow angles. Using a cutoff of 113 mm^3 , ACV had 88.29% sensitivity and 88.19% specificity in detecting narrow angles (Shaffer grade ≤ 1). AOD500, angle opening distance at 500 μm from the scleral spur; TISA500, trabecular-iris space area at 500 μm from the scleral spur; ACV, anterior chamber volume using Scheimpflug imaging; ACD, anterior chamber depth using Scheimpflug imaging.

(95% CI, 97.7–99.9). For detecting PACG (using a population prevalence of 0.88%³¹), the PPV was 7.1% (95% CI, 1.0–23.9) and the NPV was 99.9% (95% CI, 98.1–99.7). At the cutoff of 113 mm^3 , ACV had a positive LR of 8.63 (95% CI, 7.4–10.0) and a negative LR of 0.11 (95% CI, 0.03–0.4) for detecting narrow angles.

We also used another definition for narrow angles as grade ≤ 2 in all quadrants. Using this definition, ACV had an AUC of 0.901 and an 89.1% sensitivity and 87.2% specificity in detecting narrow angles. (95% CI, 0.822–0.931). Again ACV (AUC = 0.901) outperformed AOD500 nasal (AUC = 0.761; 95% CI, 0.685–0.761; $P < 0.001$), AOD500 temporal (AUC = 0.788; 95% CI, 0.722–0.814; $P < 0.001$), TISA500 nasal (AUC = 0.726; 95% CI, 0.664–0.798; $P < 0.001$), and TISA500 temporal (AUC = 0.722; 95% CI, 0.676–0.787; $P < 0.001$) in detecting narrow angles, but was similar to ACD (AUC = 0.864; 95% CI, 0.815–0.907).

Discussion

The ideal community-based screening test should not only be clinician-independent, quick and non-invasive, with a high specificity and sensitivity but also be practical and of an affordable cost. Several authors have compared ASOCT with gonioscopy as the reference and have shown sensitivities of upto 98% in detecting narrow angles.^{32,33}

Table 3 Sensitivity, specificity, positive predictive value (PPV), negative predictive value (NPV), for Scheimpflug imaging and SD-ASOCT parameters compared with gonioscopy for identifying narrow angles and area under the receiver operating characteristic curve (AUC) for parameters measured with Scheimpflug imaging and SD-ASOCT in detecting narrow angles using gonioscopy as the reference standard

Parameter	Criterion	Sensitivity (95% CI)	Specificity (95% CI)	+ LR (95% CI)	- LR (95% CI)	PPV (95% CI)	NPV (95% CI)	AUC	SE	95% CI
ACV	≤113 mm ³	90 (71.7–97.6)	88.19 (83.4–92)	8.63 (7.4–10)	0.11 (0.03–0.4)	42.9 (27.7–59)	99.0 (96.6–99.9)	0.935	0.016	0.898–0.961
ACD	≤2.45 mm	89.29 (71.8–97.6)	72.57 (66.4–78.1)	3.9 (3.4–4.4)	0.07 (0.01–0.5)	25.3 (16–36.7)	99.4 (96.8–99.9)	0.880	0.025	0.835–0.917
AOD500 nasal	≤0.34 mm	78.57 (59.0–91.7)	71.31 (65.1–77)	2.78 (2.1–3.6)	0.34 (0.2–0.8)	19.5 (11.3–30.1)	97.1 (93.4–99)	0.761	0.040	0.705–0.811
AOD500 temporal	≤0.32 mm	67.86 (47.7–84.1)	88.19 (83.4–92.0)	5.75 (4–8.2)	0.45 (0.2–0.9)	33.3 (18.6–51)	96.3 (92.8–98.4)	0.808	0.035	0.755–0.854
TISA500 nasal	≤0.2 mm ²	64.29 (44.1–81.3)	78.7 (72.8–83.8)	2.58 (1.7–3.9)	0.57 (0.1–1)	18.3 (9.5–30.4)	95.3 (91.2–97.8)	0.756	0.040	0.7–0.807
TISA500 temporal	≤0.21 mm ²	71.43 (51.3–86.7)	81.01 (75.4–85.8)	3.4 (2.4–4.7)	0.43 (0.2–0.8)	22.8 (12.8–35.8)	96.4 (92.7–98.5)	0.738	0.042	0.681–0.79

Abbreviations: ACD, anterior chamber depth; ACV, anterior chamber volume; AOD500, angle opening distance at 500 μm from the scleral spur; AUC, area under the receiver operating characteristic curve; CI, confidence interval; + LR, positive likelihood ratio; - LR, negative likelihood ratio; NPV, negative predictive value; PPV, positive predictive value; SE, standard error of the area; TISA500, trabecular-iris space area at 500 μm from the scleral spur.

Angle classification in ASOCT hinges on accurate localization of the scleral spur,³⁴ as it is used as the reference point for the relative position of trabecular meshwork. Localization of the scleral spur can be difficult, with closed angles and in the superior and inferior angles.^{7,16} Even with identical criteria, intraobserver variance in identifying the spur location can be high. In our study, the rate of undetectable sclera spur was 11.67%.

Fully automated edge detection algorithms for the ACA are being developed in an attempt to address this issue and have been described in ultrasound biomicroscopy (UBM) images,³⁵ but are not commercially available on SD-ASOCT. ACV measurements using Scheimpflug imaging are automated and do not require manual identification of the scleral spur. Kurita *et al*²⁰ recently reported that ACV had the highest discriminating ability (AUC=0.943) in screening for PAC and PAC suspects compared with UBM parameters. Using a larger sample size, we compared the diagnostic performance of ACV with SD-ASOCT angle measurements, and found that ACV had the highest discriminating ability (AUC=0.935) outperforming AOD500 and TISA500 in detecting narrow angles. We hypothesize that one of the reasons why ACV outperformed SD-ASOCT parameters is because of the ability of the rotating Scheimpflug camera to capture 50 slices through the anterior segment, and using this data to calculate ACV. Angle parameter calculations using SD-ASOCT are calculated, and are limited to single cross-sectional images of the nasal and temporal quadrants. Although in most cases this may represent the overall nature of the angle as seen gonioscopically, there are sectoral variations in eyes with uneven angle configuration,¹⁷ which will be missed on single SD-ASOCT images.

Our study has several limitations. The study group was not population based and had a relatively small sample size of 265 eyes, limited to Indian eyes. Validating these findings in a more diverse population-based study would be useful. For screening purposes, ideally the specificity should be in the high 90s,³⁶ a value which none of the parameters in this study achieved. Scheimpflug photography has its limitations in that it cannot fully visualize the entire angle.¹⁹ This leads to the location of the angle recess being estimated, and extrapolation of data by the Pentacam software to calculate the ACV.³⁷ Additionally, as it uses visible light to image the angle, it may lead to altered angle configuration.³⁸ Although repeatability of ACV measurements has been demonstrated with an intraclass correlation coefficient of 0.991,³⁹ there are concerns that as ACV is reported with no decimal places, it may be affected by rounding error.⁴⁰ Our results are not

applicable to the superior and inferior angle quadrants, as these were not imaged using SD-ASOCT. Also, we measured the parameters only under dark conditions and cannot report on the role of dynamic changes induced by different lighting conditions. Use of external fixation to center the iridocorneal angle in the instrument's field of view limits the precision for absolute standardization and centration. The shorter wavelength used in SD-ASOCT compared with TD-ASOCT does not adequately penetrate highly scattering tissue such as the sclera or iris, and thus may not be optimal for ACA imaging. Although the increased resolution of SD-ASOCT allows for identification of the Schwalbe's line, Schlemm's canal, and trabecular meshwork in some eyes, the depth and width of view provided by SD-ASOCT precludes imaging of the entire angle up to the iris root,^{41,19} which is most important when screening for narrow angles. Angle images acquired using the SD-ASOCT used in this study might be prone to distortion, as they are not dewarped.

Although correlations between ACV, gonioscopy grading and SD-ASOCT were statistically significant, most of them represent low ($r < 0.30$) to moderate associations ($r < 0.50$).^{42,43} The dynamic nature of the anterior chamber might be partially responsible for the low correlations as also the fact that SD-ASOCT images were captured in just one cross-section through the angle in each quadrant, which may not be representative of the entire angle configuration in that quadrant.

Evidence-based medicine guidelines have suggested the appropriateness of LR to judge the clinical utility of test results.^{44,45} The large positive LR (8.63; 95% CI, 7.4–10) suggests that an eye detected as having narrow angles using ACV ($\leq 113 \text{ mm}^3$) will have a moderate chance of having narrow angles on gonioscopy. The negative LR (0.11; 95% CI, 0.03–0.40) suggests that a negative result on ACV ($> 113 \text{ mm}^3$) could also be used with moderate confidence to rule out narrow angles. However, calculations of LRs depend on gonioscopy as the reference, and its limitations as an imperfect standard are well known. Even experienced examiners have reported to have only a moderate agreement in determining the angle width.^{46,47}

In conclusion, ACV measurements using the commercially available, automated software demonstrated a high discriminative value in screening for narrow angles. Improvement in image analysis algorithms could allow for the development of 'cutoff' points for discriminating narrow angles, or at least specific thresholds used to trigger a referral for examination. Only longitudinal prospective studies can accurately evaluate the predictive ability of these parameters by determining whether eyes classified as narrow angles, only by Scheimpflug or SD-ASOCT

imaging, are indeed at risk of developing PACG.³⁴ While keeping these limitations in mind, this study provides data demonstrating the potential for using ACV as a screening tool for narrow angles in an Asian Indian population.

Summary

What was known before

- Pentacam can be used for anterior segment imaging, anterior segment OCT can be used for angle imaging and screening for narrow angles.

What this study adds

- Anterior chamber volume measurements using pentacam can be used to screen for narrow angles and outperform spectral domain anterior segment OCT angle measurements in this regard.

Conflict of interest

The authors declare no conflict of interest.

References

- 1 Quigley HA, Broman AT. The number of people with glaucoma worldwide in 2010 and 2020. *Br J Ophthalmol* 2006; **90**: 262–267.
- 2 Congdon N, Wang F, Tielsch JM. Issues in the epidemiology and population-based screening of primary angle-closure glaucoma. *Surv Ophthalmol* 1992; **36**: 411–423.
- 3 Foster PJ, Baasanhu J, Alsbirk PH, Munkhbayar D, Uranchimeg D, Johnson GJ. Glaucoma in Mongolia. A population-based survey in Hovsgol province, northern Mongolia. *Arch Ophthalmol* 1996; **114**: 1235–1241.
- 4 Quigley HA, Congdon NG, Friedman DS. Glaucoma in China (and worldwide): changes in established thinking will decrease preventable blindness. *Br J Ophthalmol* 2001; **85**: 1271–1272.
- 5 He M, Foster PJ, Ge J, Huang W, Zheng Y, Friedman DS *et al*. Prevalence and clinical characteristics of glaucoma in adult Chinese: a population-based study in Liwan District, Guangzhou. *Invest Ophthalmol Vis Sci* 2006; **47**: 2782–2788.
- 6 Jacob A, Thomas R, Koshi SP, Braganza A, Muliylil J. Prevalence of primary glaucoma in an urban South Indian population. *Indian J Ophthalmol* 1998; **46**: 81–86.
- 7 Nolan WP, See JL, Chew PTK, Friedman DS, Smith SD, Radhakrishnan S *et al*. Detection of primary angle closure using anterior segment optical coherence tomography in Asian eyes. *Ophthalmology* 2007; **114**: 33–39.
- 8 Radhakrishnan S, Rollins AM, Roth JE, Yazdanfar S, Westphal V, Bardenstein DS *et al*. Real-time optical coherence tomography of the anterior segment at 1310 nm. *Arch Ophthalmol* 2001; **119**: 1179–1185.
- 9 Pekmezci M, Porco T, Lin SC. Anterior segment optical coherence tomography as a screening tool for the assessment of the anterior segment angle. *Ophthalmic Surg Lasers Imaging* 2009; **40**: 389–398.
- 10 Hoerauf H, Scholz C, Koch P, Engelhardt R, Laqua H, Birngruber R. Transscleral optical coherence tomography: a

- new imaging method for the anterior segment of the eye. *Arch Ophthalmol* 2002; **120**: 816–819.
- 11 Leung CK, Li H, Weinreb RN, Liu J, Cheung CY, Lai RY *et al*. Anterior chamber angle measurement with anterior segment optical coherence tomography: a comparison between slit lamp OCT and Visante OCT. *Invest Ophthalmol Vis Sci* 2008; **49**: 3469–3474.
 - 12 Radhakrishnan S, See J, Smith SD, Nolan WP, Ce Z, Friedman DS *et al*. Reproducibility of anterior chamber angle measurements obtained with anterior segment optical coherence tomography. *Invest Ophthalmol Vis Sci* 2007; **48**: 3683–3688.
 - 13 Sakata LM, Lavanya R, Friedman DS, Aung HT, Gao H, Kumar RS *et al*. Comparison of gonioscopy and anterior segment ocular coherence tomography in detecting angle closure in different quadrants of the anterior chamber angle. *Ophthalmology* 2008; **115**: 769–774.
 - 14 Sakata LM, Lavanya R, Friedman DS, Aung HT, Seah SK, Foster PJ *et al*. Assessment of the scleral spur in anterior segment optical coherence tomography images. *Arch Ophthalmol* 2008; **126**: 181–185.
 - 15 Wirbelauer C, Karandish A, Haberle H, Pham DT. Noncontact gonimetry with optical coherence tomography. *Arch Ophthalmol* 2005; **123**: 179–185.
 - 16 Radhakrishnan S, Goldsmith J, Huang D, Westphal V, Dueker DK, Rollins AM *et al*. Comparison of optical coherence tomography and ultrasound biomicroscopy for detection of narrow anterior chamber angles. *Arch Ophthalmol* 2005; **123**: 1053–1059.
 - 17 Asrani S, Sarunic M, Santiago C, Izatt J. Detailed visualization of the anterior segment using fourier-domain optical coherence tomography. *Arch Ophthalmol* 2008; **126**: 765–771.
 - 18 Jose Luiz Branco R, Yan L, David H. Clinical and research applications of anterior segment optical coherence tomography; a review. *Clin Experiment Ophthalmol* 2009; **37**: 81–89.
 - 19 Friedman DS, He M. Anterior chamber angle assessment techniques. *Surv Ophthalmol* 2007; **53**: 250–273.
 - 20 Kurita N, Mayama C, Tomidokoro A, Aihara M, Araie M. Potential of the pentacam in screening for primary angle closure and primary angle closure suspect. *J Glaucoma* 2009; **18**: 506–512.
 - 21 Oculus. *Pentacam Instruction Manual: Measurement and Evaluation System for the Anterior Eye Segment*. Oculus: Wetzlar, Germany, 2008.
 - 22 Sakata LM, Wong TTL, Wong HT, Kumar RS, Htoon HM, Aung HT *et al*. Comparison of Visante and slit-lamp anterior segment optical coherence tomography in imaging the anterior chamber angle. *Eye* 2009; **24**(4): 578–587.
 - 23 Pavlin CJ, Harasiewicz K, Foster FS. Ultrasound biomicroscopy of anterior segment structures in normal and glaucomatous eyes. *Am J Ophthalmol* 1992; **113**: 381–389.
 - 24 Shaffer RN. A new classification of the glaucomas. *Trans Am Ophthalmol Soc* 1960; **58**: 219–225.
 - 25 Shaffer RN. A suggested anatomic classification to define the pupillary block glaucomas. *Invest Ophthalmol* 1973; **12**: 540–542.
 - 26 Shaffer RN. Primary glaucomas. Gonioscopy, ophthalmoscopy and perimetry. *Trans Am Acad Ophthalmol Otolaryngol* 1960; **64**: 112–127.
 - 27 DeLong ER, DeLong DM, Clarke-Pearson DL. Comparing the areas under two or more correlated receiver operating characteristic curves: a nonparametric approach. *Biometrics* 1988; **44**: 837–845.
 - 28 Perkins NJ, Schisterman EF. The inconsistency of ‘Optimal’ cutpoints obtained using two criteria based on the receiver operating characteristic curve. *Am J Epidemiol* 2006; **163**: 670–675.
 - 29 Youden WJ. Index for rating diagnostic tests. *Cancer* 1950; **3**: 32–35.
 - 30 Hilden J, Glasziou P. Regret graphs, diagnostic uncertainty and Youden’s index. *Stat Med* 1996; **15**: 969–986.
 - 31 Vijaya L, George R, Arvind H, Baskaran M, Ve Ramesh S, Raju P *et al*. Prevalence of primary angle-closure disease in an urban south Indian population and comparison with a rural population: the chennai glaucoma study. *Ophthalmology* 2008; **115**: 655–660.
 - 32 Karandish A, Wirbelauer C, Haberle H, Pham DT. Reproducibility of gonimetry with slitlamp-adapted optical coherence tomography. *Ophthalmologie* 2004; **101**: 608–613.
 - 33 See JLS, Chew PTK, Smith SD, Nolan WP, Chan YH, Huang D *et al*. Changes in anterior segment morphology in response to illumination and after laser iridotomy in Asian eyes: an anterior segment OCT study. *Br J Ophthalmol* 2007; **91**: 1485–1489.
 - 34 Thomas R. Anterior segment optical coherence tomography. *Ophthalmology* 2007; **114**: 2362–2363.
 - 35 Leung CK, Yung WH, Yiu CK, Lam SW, Leung DY, Tse RK *et al*. Novel approach for anterior chamber angle analysis: anterior chamber angle detection with edge measurement and identification algorithm (ACADEMIA). *Arch Ophthalmol* 2006; **124**: 1395–1401.
 - 36 Stamper RL. Glaucoma screening. *J Glaucoma* 1998; **7**: 149–150.
 - 37 Fukuda S, Kawana K, Yasuno Y, Oshika T. Anterior ocular biometry using 3-dimensional optical coherence tomography. *Ophthalmology* 2009; **116**: 882–889.
 - 38 Friedman DS, Gazzard G, Min CB, Broman AT, Quigley H, Tielsch J *et al*. Age and sex variation in angle findings among normal Chinese subjects: a comparison of UBM, scheimpflug, and gonioscopic assessment of the anterior chamber angle. *J Glaucoma* 2008; **17**: 5–10.
 - 39 Georgios L, Maria G, Andreas K, Michael F, Efstratios A, Vassilios K. Anterior chamber volume measurements with Visante optical coherence tomography and Pentacam: repeatability and level of agreement. *Clin Experiment Ophthalmol* 2009; **37**: 772–774.
 - 40 Shankar H, Taranath D, Santhirathelagan CT, Pesudovs K. Anterior segment biometry with the Pentacam: comprehensive assessment of repeatability of automated measurements. *J Cataract Refract Surg* 2008; **34**: 103–113.
 - 41 Wong H-T, Lim MC, Sakata LM, Aung HT, Amerasinghe N, Friedman DS *et al*. High-definition optical coherence tomography imaging of the iridocorneal angle of the eye. *Arch Ophthalmol* 2009; **127**: 256–260.
 - 42 Kotrlík JW, Williams HA. The incorporation of effect size in information technology, learning, and performance research. *Information Technology, Learning, and Performance Journal* 2003; **21**: 1–7.
 - 43 Jacob C. *Statistical Power Analysis for the Behavioral Sciences*. Lawrence Erlbaum Associates: Hillsdale, New Jersey, 1988, p 567.
 - 44 Radack KL, Rouan G, Hedges J. The likelihood ratio. An improved measure for reporting and evaluating diagnostic test results. *Arch Pathol Lab Med* 1986; **110**: 689–693.

- 45 Jaeschke R, Guyatt GH, Sackett DL. Users' guides to the medical literature. III. How to use an article about a diagnostic test. B. What are the results and will they help me in caring for my patients? The Evidence-Based Medicine Working Group. *JAMA* 1994; **271**: 703–707.
- 46 Nolan WP, Foster PJ, Devereux JG, Uranchimeg D, Johnson GJ, Baasanhu J. YAG laser iridotomy treatment for primary angle closure in east Asian eyes. *Br J Ophthalmol* 2000; **84**: 1255–1259.
- 47 Foster PJ, Devereux JG, Alsbirk PH, Lee PS, Uranchimeg D, Machin D *et al*. Detection of gonioscopically occludable angles and primary angle closure glaucoma by estimation of limbal chamber depth in Asians: modified grading scheme. *Br J Ophthalmol* 2000; **84**: 186–192.